*Bulletin of Mathematical Biology* (2003) **65**, 519–534
doi:10.1016/S0092-8240(03)00013-2

# Traveling Waves of Infection in the Hantavirus Epidemics

G. ABRAMSON*† AND V. M. KENKRE
Center for Advanced Studies and Department of Physics and Astronomy,
University of New Mexico,
Albuquerque, NM 87131,
U.S.A.
*E-mail*: abramson@cab.cnea.gov.ar; kenkre@unm.edu

T. L. YATES
Department of Biology and Museum of Southwestern Biology,
University of New Mexico,
Albuquerque, NM 87131,
U.S.A.

R. R. PARMENTER
Sevilleta Long-term Ecological Research Program,
Department of Biology,
University of New Mexico,
Albuquerque, NM 87131,
U.S.A.

Traveling waves are analyzed in a model of the hantavirus infection in deer mice. The existence of two kinds of wave phenomena is predicted. An environmental parameter governs a transition between two regimes of propagation. In one of them the front of infection lags behind at a constant rate. In the other, fronts of susceptible and infected mice travel at the same speed, separated by a constant delay. The dependence of the delay on system parameters is analyzed numerically and through a piecewise linearization.



## 1. INTRODUCTION

Human disease caused by members of the genus Hantavirus is a persistent problem in many regions of the world (Mills *et al.*, 1999b). Each species of Hantavirus is almost exclusively associated with a single rodent reservoir, and human disease caused by these pathogens can range from mild to very severe, with a mortality rate in some cases approaching 50%. Such is the case with hantavirus pulmonary syndrome (HPS) produced by Sin Nombre virus associated with the deer mouse (*Peromyscus maniculatus*). A serious outbreak of this disease in the North American

*Author to whom correspondence should be addressed.
†Also at: Centro Atómico Bariloche and CONICET, 8400 S. C. de Bariloche, Argentina.

0092-8240/03/030519 + 16 $30.00/0 

Southwest in 1993 led to the identification of the virus (Nichol *et al.*, 1993) and its association with the deer mouse (Childs *et al.*, 1994; Parmenter *et al.*, 1993). Since then, enormous effort and resources have been devoted to understanding the ecology and epidemiology of the virus–mouse association, with the ultimate goal being prediction of human risk (Parmenter *et al.*, 1998; Mills *et al.*, 1999a).

Yates *et al.* (2002) showed that the outbreaks of HPS in the Southwest in 1993 and again in 1998–2000 were associated with the El Niño-southern oscillation (ENSO) phenomenon. The warm-phase of the ENSO (termed an 'El Niño') produced increased amounts of fall–spring precipitation in the arid and semi-arid regions of New Mexico and Arizona, which in turn initiated greater production of rodent food resources (plants, seeds, berries, nuts and insects). These abundant food resources allowed greater reproduction in rodents (the 'trophic cascade hypothesis'), and within a year, large increases in rodent densities were observed. At these high densities, rodents then began dispersing across the landscape, and came into contact with humans in homes and businesses. Within a year of the peak rodent densities, increases in density of SNV-infected rodents were observed, suggesting that a 'wave' of virus infection was following the 'wave' of rodent dispersal. The origins of both of these waves were hypothesized to be in the 'optimal habitats' or refugia located in natural canyon terrain covered by woodlands and forests.

The complete disappearance of the disease from local populations during times of adverse environmental conditions, and its eventual reappearance when conditions change (Mills *et al.*, 1999a; Parmenter *et al.*, 1999; Yates *et al.*, 2002), have been recently shown by Abramson and Kenkre (2002) to arise as a bifurcation phenomenon in a simple epidemic model. The purpose of the present paper is to analyze, in the framework of that model, the dynamics of simple traveling waves, as a mechanism by which an epidemic wave of hantavirus might propagate into a previously uninfected region.

## 2. Spatially Extended Model

The model of Abramson and Kenkre (2002) is a mean-field continuous model which has been intentionally kept simple enough to facilitate the comprehension of the basic mechanisms, and at the same time to incorporate as many facts about the ecology and epidemiology of the biological system as possible. The reader is referred to Abramson and Kenkre (2002) for a detailed discussion, which we summarize here. It is known that the virus does not affect properties such as the mortality of the mice, so that no appreciable difference in death rate, for example, is to be expected between susceptible and infected mice. It is also not transmitted to newborns, so that no mice are born in the infected state. The infection is transmitted from mouse to mouse through individual contacts, such as fights. More general facts of the ecology of *Peromyscus* indicate that adults

occasionally shift their home range to nearby locations, in particular if these are vacant (Stickel, 1968; Vessey, 1987). This enables us to model the transport of mice as a diffusion process. Finally, intra-species competition for resources indicate a saturated population growth, which has been observed to be of a logistic form in the laboratory (Terman, 1968). Logistic growth is also a well-established metaphor of the dynamics of a self-limiting population (Murray, 1993). For the sake of simplicity, assume further that the only population structure is the division of the whole population into susceptible and infected mice, denoted by $M_S$ and $M_I$ respectively, and with $M_S + M_I = M$ the total mice population. With these ingredients, the model is described by the following equations:

$$\frac{\partial M_S}{\partial t} = bM - cM_S - \frac{M_S M}{K(x,t)} - aM_S M_I + D\nabla^2 M_S, \tag{1}$$

$$\frac{\partial M_I}{\partial t} = -cM_I - \frac{M_I M}{K(x,t)} + aM_S M_I + D\nabla^2 M_S. \tag{2}$$

Observe that the carrying capacity $K(x,t)$, containing the most direct effect of the environment on the mouse population, is allowed, in our model, a spatial and a temporal variation, to accommodate for diversity of habitats and temporal phenomena. The latter comprise the yearly variation due to seasonality, but also sporadic fluctuations such as droughts and El Niño effects. The other parameters, characterizing the different processes affecting the mice, are supposed constant. The birth rate $b$ characterizes a source of susceptible mice only. The death rate, common to both subpopulations, is $c$. The contagion rate is the parameter $a$. Finally, a diffusion coefficient $D$ characterizes a diffusive transport mechanism of the mice. The rationale behind each term in equations (1) and (2) is simple, and the reader is referred to Abramson and Kenkre (2002) for a detailed discussion.

The sum of the two equations (1) and (2) reduces to a single equation for the whole population

$$\frac{\partial M}{\partial t} = (b-c)M\left(1 - \frac{M}{(b-c)K}\right) + D\nabla^2 M. \tag{3}$$

This is Fisher's equation, originally proposed as a deterministic model of the spread of a favored gene in a population (Fisher, 1937), and which eventually became a standard model for a self-regulated field in a diversity of situations (Murray, 1993; Abramson *et al.*, 2001).

In Abramson and Kenkre (2002) it was shown that, as a function of $K$, the system undergoes a bifurcation between a stable state with only susceptible mice (and $M_I = 0$) to a stable state with both positive populations. The value of the critical carrying capacity is a function of the parameters in the following way:

$$K_c = \frac{b}{a(b-c)}. \tag{4}$$

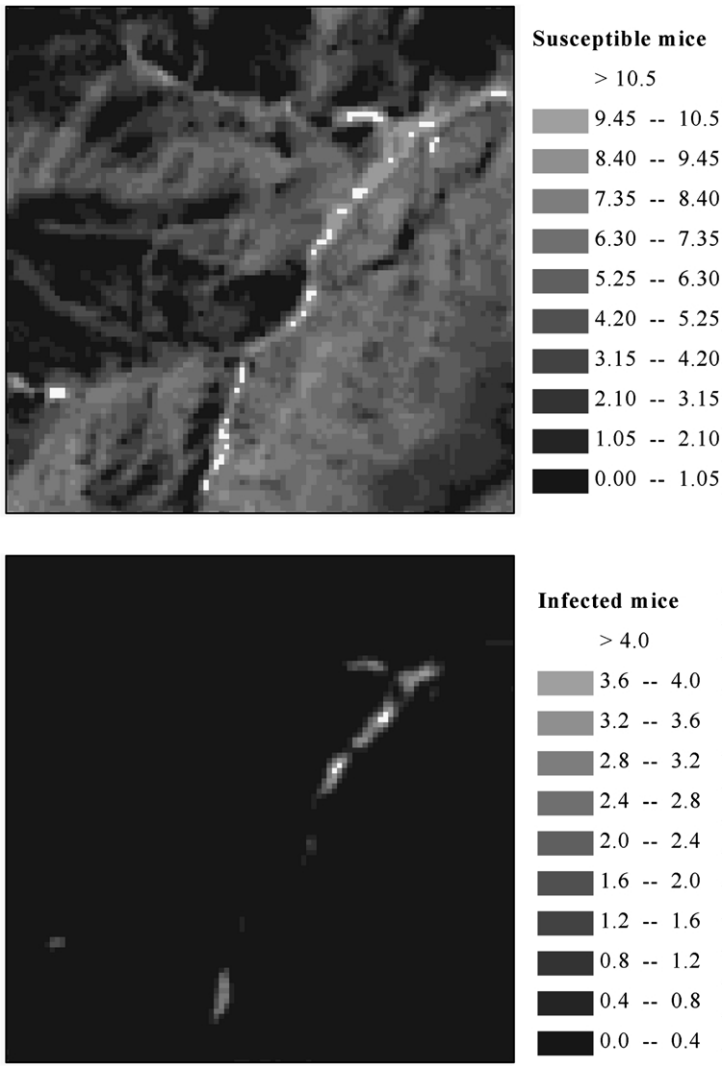


Figure 1. Density plots showing the characteristic distribution of susceptible and infected mice in an heterogeneous landscape. The carrying capacity has been modeled according to the vegetation, derived from satellite imagery. It is a realistic simulation of the kind of patterns expected in the mice distribution.

This critical value does not depend on $D$, and the same bifurcation is observed either in a space-independent system ($D = 0$) or in a homogeneous extended one in the presence of diffusion. In a non-homogeneous situation, for moderate values of the diffusion coefficient, the infected subpopulation remains restricted to those places where $K > K_c$, becoming extinct in the rest. During times of adverse environmental conditions, these regions become isolated and constitute the observed refugia. Figure 1 shows a typical situation of this phenomenon. A simulated, albeit realistic, landscape of $K(x)$ has been derived from satellite

images of a 10 km $\times$ 10 km arid landscape in Northern Patagonia. The carrying capacity is supposed proportional to the vegetation cover, and, as may be clearly inferred from the density plots, turns out to be highest along a river. The density plots show the distribution of the populations of susceptible and infected mice. It can be seen that susceptible mice cover most of the range. Meanwhile, the infected population has become extinct in most of it, and persists only in some of the places of highest $K$. The distributions shown in Fig. 1 constitute a stable equilibrium of the system, found by numerical resolution of equations (1) and (2) from an arbitrary initial condition, and with zero-current boundary conditions. This stationary situation is a realistic representation of the kind of mice distribution to be expected in the wild.

## 3. TRAVELING WAVES

When conditions in the landscape change, how do the infected phase evolve from the refugia, retracting from or, more importantly, invading previously uninfected regions? This is the primary question we address in the present paper. Fisher's equation (3) has found wide applicability for the description of the formation and propagation of spatio-temporal patterns. Traveling wave solutions of Fisher's equation paradigmatically show how a stable phase 'invades' an unstable one in the form of a front, propagating at a certain speed. Needless to say, the speed of this propagating front is not the speed of the individual mice: the mice move diffusively. The diffusion just provides a local coupling mechanism for the populations between adjacent regions. It is the (nonlinear) growth of the population which is responsible for developing and sustaining the shape of the front, and propagating the more stable equilibrium at the expense of the less stable one. We will show, in the following, that a 'wave of infection' arises in a similar way in our model. It is worthwhile to note that this wave of infection is not a moving population of infected mice, but actually a spatial pattern of the distribution of the infection in the mouse population, propagating as a wave through the conversion of part of the susceptible mice into infected ones, as they come into contact with other infected rodents.

There is no reason to suppose *a priori* that the two waves, susceptible and infective, will travel at the same speed. Accordingly, we use an ansatz which incorporates two independent traveling waves. In one dimension, $z_1 = x - v_S t$ in equation (1) and $z_2 = x - v_I t$ in equation (2). This gives the following second-order system of ordinary differential equations:

$$D\frac{d^2 M_S(z_1)}{dz_1^2} + v_S\frac{dM_S(z_1)}{dz_1} + f(M_S, M_I) = 0, \tag{5}$$

$$D\frac{d^2 M_I(z_2)}{dz_2^2} + v_I\frac{dM_I(z_2)}{dz_2} + g(M_S, M_I) = 0, \tag{6}$$

where $v_S$ and $v_I$ are the speeds of the susceptible and infected waves respectively, and $f$ and $g$ are the non-diffusive terms in (1)–(2).

There are two interesting scenarios for these waves. In the first one, a large part of the system is initially at a state of low carrying capacity, below $K_c$, and consequently the population consists of uninfected mice only, at the stable equilibrium. Let us suppose that this region is in contact with a refugium. If environmental changes occur, and the whole region finds itself at a value of the carrying capacity $K > K_c$, the population will be out of equilibrium. Two processes will occur simultaneously: the population of susceptible mice will evolve towards a new equilibrium, and a wave of infected mice will advance from the refugium, invading the susceptible population. The speed of this wave can be calculated from the stability analysis of the equilibrium states, requiring that the unstable infected rodent density does not oscillate below zero. This unstable equilibrium is $M_S^* = K(b-c)$, $M_I^* = 0$, and a linear stability analysis of the system (5)–(6) provides the following four eigenvalues:

$$\lambda_{1,2} = \frac{-v \pm \sqrt{v^2 + 4D(b-c)}}{2D}, \tag{7}$$

$$\lambda_{3,4} = \frac{-v \pm \sqrt{v^2 + 4D[b - aK(b-c)]}}{2D}. \tag{8}$$

The requirement that $M_I(z)$ does not oscillate below 0 imposes a restriction to the radical in equation (8), from which we find the following expression for the speed of the traveling wave:

$$v \geq 2\sqrt{D[-b + aK(b-c)]}. \tag{9}$$

An example of such a wave is shown in Fig. 2(a), found by a numerical integration of equations (1) and (2) in one dimension.

The second interesting scenario corresponds to a system which is initially empty of mice. This situation is always unstable within the validity of our simple model, but it is certainly a biological possibility. Consider a system with $K > K_c$, and with $M_S = M_I = 0$ in almost all of its range, but in contact with a refugium in equilibrium, that is, a small region where $M_S = M_S^* > 0$ and $M_I = M_I^* > 0$. A wave of both mice populations will develop and invade the empty region. In fact, the total population will display the behavior of a traveling wave of Fisher's equation. The propagating front will consist only of susceptible mice at the leading edge, because the population is expanding into a region free of rodents. The population of infected mice needs a substrate of susceptible mice to grow and, in consequence, a front of infected population will travel 'within' the susceptible front, where a population of susceptible is already established. A certain delay or lag exists between the leading edges of the two fronts. The magnitude of this delay depends on the parameters of the system. A typical situation is shown in Fig. 2(b),

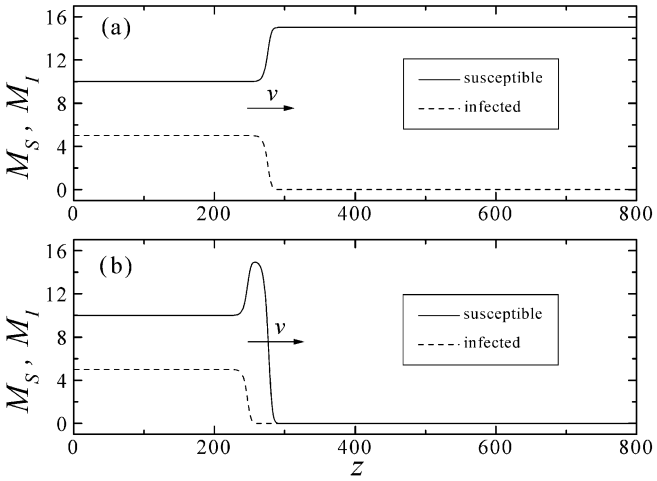


Figure 2. Traveling waves in the one-dimensional model. (a) Infection wave invading a noninfected population; (b) noninfected mice invading an empty region, followed by an infection wave. Model parameters: $a = 0.1$, $b = 1$, $c = 0.5$, $D = 1$, $K = 30$. Both waves move at the same speed $v = \sqrt{2}$ for this choice of parameters.

where the susceptible population is shown as a continuous line and the infected as a dashed one. Both fronts move to the right, the infected one lagging behind the susceptible. Once the front has passed, both populations stabilize at the equilibrium values $M_S^*$ and $M_I^*$. In other words, observing a fixed point in space one would see, as the front passes by, the population growing from its unstable zero state to the stable one. As before, we can find the speeds of these two waves from a stability analysis around the corresponding equilibria. The leading wave propagates into the null equilibrium, $M_S^* = M_I^* = 0$, to which the following eigenvalues correspond:

$$\mu_{1,2} = \frac{-v_I \pm \sqrt{v_I^2 + 4Dc}}{2D}, \tag{10}$$

$$\mu_{3,4} = \frac{-v_S \pm \sqrt{v_S^2 - 4D(b-c)}}{2D}. \tag{11}$$

In this situations, we require that $M_S(z)$ does not oscillate below 0, and equation (11) provides the restriction on the speed of the susceptible front:

$$v_S \geq 2\sqrt{D(b-c)}, \tag{12}$$

which is, naturally, the same result as for Fisher's equation. The second front, developed when part of the quasi-stable population of susceptible mice is converted into infected, evolves from the equilibrium $M_S^* = K(b-c)$, $M_I^* = 0$, as in the previous scenario. Consequently, the same linear stability analysis applies, and

from equation (8) we find a speed analogous to equation (9). The front of infected mice moves behind the susceptible one at a speed

$$v_I \geq 2\sqrt{D[-b + aK(b-c)]}, \tag{13}$$

which, unlike $v_S$, *does* depend on the contagion rate $a$ and the carrying capacity $K$. Figure 2(b) shows such a situation. The density of susceptible mice rises from zero and lingers near the positive unstable equilibrium before tending to the stable one. It is remarkable that a delay exists between the two fronts, even when no such effect was explicitly considered in the dynamics (such as incubation time, or age dependence). Such delays have been observed in some populations and rationalized in different ways [see Ernest *et al.* (2000) or Mills *et al.* (1999a) for a synthesis].

Even though equations (9), (12) and (13) give only a lower bound to the speed of propagation of the fronts, and allow a continuum of speeds above this, in real situations only the lower bound is expected to be observed as a stationary solution. Higher speeds may, however, play a role in transient situations: their relevance cannot be underestimated in far-from-equilibrium systems such as real mice in the wild, subject to a fluctuating environment.

The different functional dependence of $v_S$ and $v_I$ on the parameters of the system [equations (12) and (13)] indicates that two regimes are possible. Indeed, when $v_I < v_S$ the front of infection lags behind the front of susceptible at a delay $\Delta$ that increases linearly in time: $\Delta(t) = (v_S - v_I)t$. Elementary manipulation of equations (12) and (13) shows that this occurs whenever the carrying capacity satisfies

$$K_c < K < K_0 \equiv \frac{2b - c}{a(b - c)} \tag{14}$$

where $K_0$ is a new critical carrying capacity. At $K = K_0$ the delay becomes effectively constant. For values of $K$ greater than $K_0$, the velocities $v_I$ and $v_S$, calculated from linear considerations around the equilibria, satisfy $v_I > v_S$. This regime is clearly unphysical in a stationary situation, since the front of susceptible mice necessarily precedes the infected one. It could be realizable and relevant in transient situations, that will be analyzed elsewhere. From numerical resolution of the system, we can observe that $v_I \to v_S$ and the delay tends to a constant value, whenever $K > K_0$. Figure 3 shows the temporal evolution of the delay in the two regimes $K < K_0$ and $K > K_0$, as well as in the critical case $K = K_0$, where it is seen to increase as $\Delta \sim t^{1/4}$. It can be seen that there is a transient time in both regimes, that gets progressively longer as $K$ approaches $K_0$ either from above or from below.

This critical slowing down, characteristic of many dynamical processes near the critical point, forces to use care in the numerical solution of the system. The results shown in Figs 3 and 4 were obtained in the following way. The space variable of equations (1) and (2) is discretized and the system reduces to a grid of $N$ nodes.

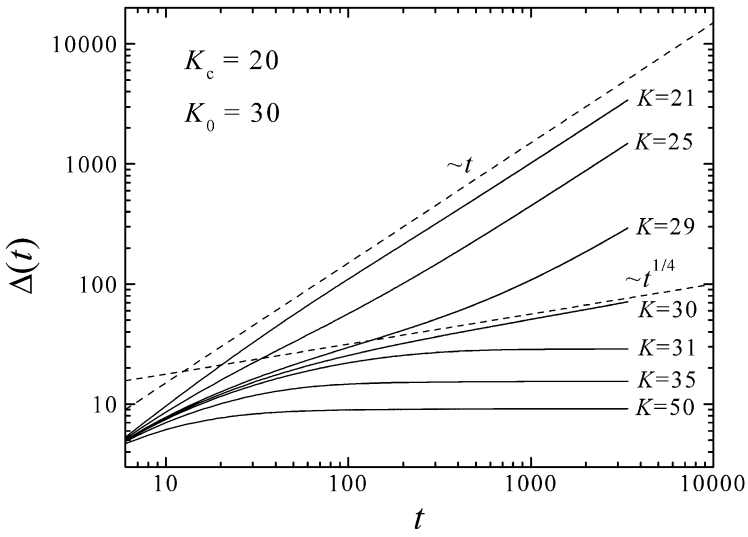


Figure 3. Delay of the infected front, as a function of time, following an initial condition as described in the text. Two regimes are shown: $K_c < K < K_0$ and $K_0 < K$, separated by the critical case $K = K_0$, that behaves asymptotically as $t^{1/4}$. The system used for the numerical integration is based on a grid with 2000 nodes. Other system parameters are $b = 1$, $c = 0.5$, $D = 1$.

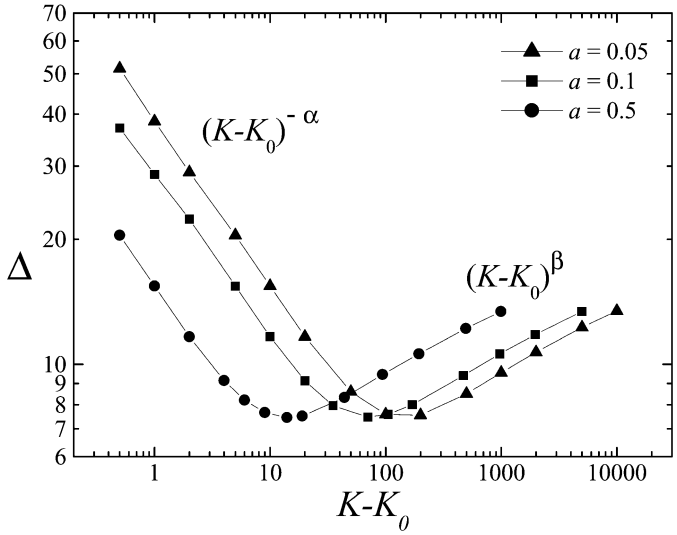


Figure 4. Delay of the infected front, as a function of $K$. Three infection rates are shown, as indicated in the legend. The other system parameters are $b = 1$, $c = 0.5$, $D = 1$. The system size is $N = 2000$ for most of the calculations, and $N = 20\,000$ for the leftmost three. The resulting averaged exponents are $\alpha = 0.388 \pm 0.005$ and $\beta = 0.16 \pm 0.02$.

For the analysis of the scenarios of wave propagation mentioned above, border conditions are taken fixed at the values of the equilibrium states of interest: positive infected at the left border, zero infected at the right border. A simple discretization of the second derivative provides the diffusive transport through near-neighbors coupling. A fourth-order Runge–Kutta is then implemented on each node of the grid, providing the numerical integration in time. Time steps ranging from 0.5 to 0.001 were tried, without observing any noticeable difference in the solutions. Most of the results we show were obtained with systems of size $N = 2000$. We have checked the consistency of these results with systems of up to $N = 20\,000$, which enables longer integration times before the infection reaches the right border. Results very near the critical point were obtained with these larger systems, checking for the stabilization of a stationary regime. The delay $\Delta$ between the two fronts is found, within this procedure, using the same definition as the one used in the Appendix: let $M_S^*$ and $M_I^*$ be the nontrivial (positive) equilibria, found on the left-hand side of the system; then $x_S(t)$ and $x_I(t)$ are defined as the instantaneous positions of the fronts, such that $M_S(x_S) = M_S^*/2$ and $M_I(x_I) = M_I^*/2$, respectively. The delay is then calculated as $\Delta(t) = x_S(t) - x_I(t)$, and its asymptotic value $\Delta$ is found through the fitting of an appropriate function to it.

With the assumption that $v_S = v_I = v$, it is possible to perform a piecewise linearization of equations (5) and (6) and find an approximate analytical expression for the front shapes shown in Fig. 2(b) and, consequently, for the delay $\Delta$ in the stationary state. The details of the calculation can be found in the Appendix. The main result is the following expression for the delay, for the case of equal speeds of the two classes of mice:

$$\Delta = \frac{\sqrt{D}}{i\sqrt{(b-c)a(K-K_0)}} \log(w_1 w_2), \tag{15}$$

where $w_1$ and $w_2$ are complex numbers of unit modulus that depend on $a$, $b$ and $c$, so that the logarithm is effectively twice the phase difference between them. When $K \to K_0^+$, the arguments of $w_1$ and $w_2$ tend to $\pi$ and 0 respectively, so that the following critical behavior is predicted by the linear approximation

$$\Delta \sim \sqrt{D}[(b-c)a(K-K_0)]^{-1/2}, \qquad \text{when } K \to K_0^+. \tag{16}$$

We have analyzed the dependence of $\Delta$ on $K$ by means of numerical resolution of the full system. In Fig. 4 we plot the asymptotic value of $\Delta$ as a function of $K - K_0$ for a variety of system parameters. The behavior is found to be

$$\Delta \sim \sqrt{D}[(b-c)a(K-K_0)]^{-\alpha} \tag{17}$$

for a range of values of $K$ immediately above $K_0$. The exponent $\alpha$ is parameter independent. From the power-law regime of Fig. 4, and averaging for several values of $a$ in the range 0.05–0.5, we have $\alpha = 0.388 \pm 0.005$. This value corresponds to $K - K_0$ covering more than an order of magnitude. The slowing

down of the dynamics near the critical point, unfortunately, makes the analysis of situations with values of $K - K_0$ smaller than those shown in Fig. 4 increasingly difficult, since a stationary state could not be achieved. There is a discrepancy in the exponent found numerically in the fully nonlinear system and the one found in the linearized approximation, which shows the limitation of the linearized solution.

This critical behavior of the delay persists while the wavefronts are of the kind shown in Fig. 2(b). However, if $K$ continues to grow the equilibrium value of the infected population turns greater than the equilibrium value of the susceptible. There is a gradual crossover to a situation where most of the population becomes infected. The value of the carrying capacity at which this happens can be estimated from the known equilibria, $M_S^* = M_I^*$, giving

$$K_1 = \frac{2b}{a(b-c)}. \tag{18}$$

Indeed, the numerical results show that the power law decay of the delay as a function of $K$ starts to flatten for values of $K > K_1$ and reaches a minimum which shows the same $a^{-1}$ dependence that $K_1$ does. One might conjecture that greater values of $K$ are probably unrealistic in the southwest, where the sporadic disappearance of the infected population is an indication that the carrying capacity lies near the critical one, $K_c$. It is nevertheless interesting to point out that the interaction of the two fronts in this regime results in an *increase* of the delay as a function of $K$. This increase is also algebraic:

$$\Delta \sim (K - K_0)^{\beta}, \tag{19}$$

with $\beta \approx 0.16 \pm 0.02$, as found in the numerical calculations.

## 4. CONCLUSION

We have analyzed the propagation of traveling fronts in a simple one-dimensional model of the ecology and epidemiology of the hantavirus in deer mouse. In our model, the populations of susceptible and infected mice are dynamically governed by processes that simply, yet realistically, describe known facts of the rodent population. These processes are described by nonlinear terms in the evolution equations. The movement of the mice is modeled by a diffusive term, that provides for coupling of the populations in neighboring regions of space. The interaction of the nonlinear growth with the diffusion provides a mechanism for the formation of stable traveling waves in the form of fronts. We have found that, when a mouse-free region is in contact with an infected region in equilibrium, two front waves propagate into the empty region. The first one is a wave of susceptible mice. At the leading edge of this wave, the population is composed of susceptible mice only. Since the infected population can only develop and persist within

a susceptible one, the wave of infected mice propagates within the wave of the susceptible population. The leading edge of the infection wave, developing from the susceptible population, follows the leading edge of the susceptible wave with a certain delay, as exemplified in Fig. 2(b). Both waves move deterministically at a speed dictated by the parameters of the system. While this speed depends on the diffusion coefficient, it is not the speed of individual mice. Two regimes of propagation exist, controlled by the environmental parameter $K$. If $K_c < K < K_0$, the lag between the two fronts increases linearly in time. Conversely, if $K > K_0$, the two fronts propagate at the same speed and the delay depends critically on the difference $K - K_0$.

The occurrence of this double regime may be of relevance for the control of the propagation of an epidemic wave. Indeed, the controlled reduction of $K$ ahead of a propagating wave seems the most effective mean of stopping or reducing its advance. Ideally, the carrying capacity should be reduced below $K_0$, to ensure the complete extinction of the infection. However, if such a reduction is not feasible, the fact that $K_0 > K_c$ provides an alternative: a reduction of the carrying capacity below $K_0$ would make the wave of infection start to lag more and more behind the wave of healthy mice. Possible implementations of these strategies, based on the propagation of waves in the presence of 'barriers', will be analyzed in detail elsewhere.

The existence of dynamical phenomena such as these traveling fronts also opens the interesting possibility of subjecting our predictions to experimental verification. Controlled experiments of front propagation could be possible in the Sevilleta LTER facility, that the University of New Mexico operates near Socorro, NM (Sevilleta Long-Term Ecological Research Program, http://sevilleta.unm.edu), especially in the 16-hectare rodent enclosure there. Measurements of uncontrolled mice populations along lines radiating from the refugia of infection will also provide evidence of the propagation mechanisms where long-term measurements can be taken in light of climate and rodent population density fluctuations. The observation of these in real mice populations will provide a valuable source of data to assign realistic values to the parameters of the mathematical model.

## ACKNOWLEDGEMENTS

We thank Fred Koster, Jorge Salazar, Greg Glass, Karl Johnson, Luca Giuggioli and María Alejandra Aguirre for many useful discussions. Financial support for the study was partially provided by the Consortium of the Americas for Interdisciplinary Science under a contract from the Los Alamos National Laboratory to the University of New Mexico and a grant from the National Science Foundation's Division of Materials Research (DMR0097204). A part of the numerically intensive computations was carried out at the Albuquerque High Performance Computing Center facilities.

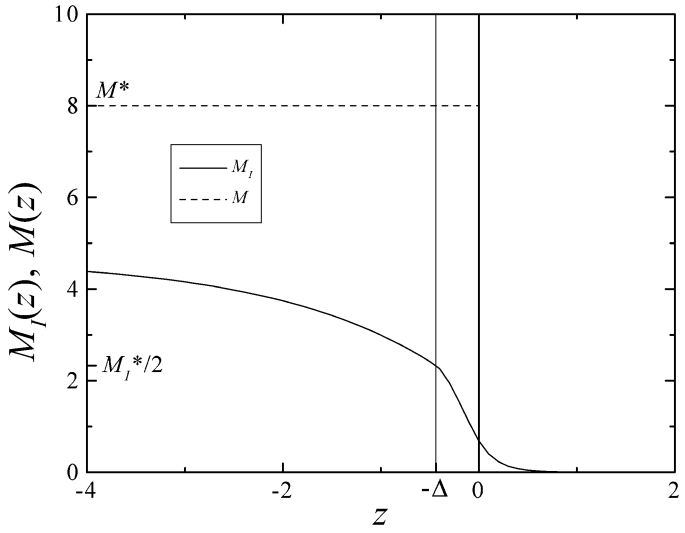


Figure 5. Linearized solutions. System parameters are: $a = 0.3$, $b = 1$, $c = 0.5$, $K = 16$, $D = 0.1$.

## APPENDIX: LINEARIZED SOLUTIONS

For the purpose of finding approximate solutions of the waves profiles, it is better to replace the system (5)–(6) with one involving $M$ and $M_I$ instead:

$$DM'' + vM' + (b - c)M - \frac{M^2}{K} = 0, \tag{A.1}$$

$$DM_I'' + vM_I' + q(M)M_I - aM_I^2 = 0, \tag{A.2}$$

where $q(M(z)) = -c + aM(z) - M(z)/K$ and both speeds are assumed equal, as observed in numerical resolutions for the regime $K > K_0$. Primes denote differentiation with respect to $z$. The reason for using this system is that the equation for $M(z)$, equation (A.1), being closed, can be solved independently of $M_I$. Its solution can be used then into equation (A.2) as a $z$-dependent parameter and solve for $M_I(z)$.

Linearized solutions for the traveling waves of Fisher's equation (A.1) are well known, and essentially consist of two exponentials, matched smoothly at $z = 0$, representing a front that travels to the right at a speed $v \geq 2\sqrt{D(b-c)}$. Such a function needs a further simplification in order to solve equation (A.2). We approximate $M(z)$ with a step function discontinuous at $z = 0$: $M(z) = M^* = K(b - c)$ if $z < 0$ and $M(z) = 0$ if $z > 0$. Consequently, we have that $q(z) = aM_I^* = -b + aK(b - c)$ if $z < 0$ and $q(z) = -c$ if $z > 0$. We also linearize on both sides of the center value $M_I(-\Delta) = M_I^*/2$, which defines $\Delta$ as the delay between the two waves. Figure 5 shows the geometry of the procedure.

The linearized equation for $M_I$ breaks into three regimes:

$$DM_I'' + vM_I' - a(M_I - M_I^*) = 0 \qquad \text{if } z < -\Delta, \tag{A.3}$$

$$DM_I'' + vM_I' + aM_I^* M_I = 0 \qquad \text{if } z \in [-\Delta, 0], \tag{A.4}$$

$$DM_I'' + vM_I' - CM_I = 0 \qquad \text{if } 0 < z. \tag{A.5}$$

The solutions of these are respectively

$$M_1(z) = -\frac{b}{a} + K(b-c) + a_1 e^{\lambda z} \qquad \text{if } z < -\Delta, \tag{A.6}$$

$$M_2(z) = b_1 e^{\mu_+ z} + b_2 e^{\mu_- z} \qquad \text{if } z \in [-\Delta, 0], \tag{A.7}$$

$$M_3(z) = c_1 e^{\nu z} \qquad \text{if } 0 < z, \tag{A.8}$$

where

$$\lambda = \frac{\sqrt{b-c+a} - \sqrt{b-c}}{\sqrt{D}}, \tag{A.9}$$

$$\mu_\pm = -\sqrt{\frac{b-c}{D}} \pm i\sqrt{\frac{b-c}{D}a(K-K_0)}, \tag{A.10}$$

$$\nu = -\frac{\sqrt{b-c} + \sqrt{b}}{\sqrt{D}}, \tag{A.11}$$

and the terms that diverge in infinity have already been cancelled. It is clear that $\lambda > 0$ and $\nu < 0$, as required for the solution not to diverge in $\mp\infty$. The real part of $\mu_\pm$ is always positive, and there is an imaginary part when $K > K_0$.

The solutions $M_1$, $M_2$ and $M_3$ need to be matched smoothly at $z = -\Delta$ and 0, in the following way ($r = b - c$ from now on):

$$M_1(-\Delta) = -\frac{b}{2a} + \frac{kr}{2}, \tag{A.12}$$

$$M_2(-\Delta) = -\frac{b}{2a} + \frac{kr}{2}, \tag{A.13}$$

$$M_1'(-\Delta) = M_2'(-\Delta), \tag{A.14}$$

$$M_2(0) = M_3(0), \tag{A.15}$$

$$M_2'(0) = M_3'(0). \tag{A.16}$$

These are five equations with five unknowns that can be solved without difficulty:

$$a_1 = -\frac{-b/a + kr}{2} e^{\lambda\Delta}, \tag{A.17}$$

$$b_1 = -\frac{(\lambda + \mu_-)}{2(\mu_+ - \mu_-)}(kr - b/a)e^{\mu_+ \Delta}, \tag{A.18}$$

$$b_2 = -\frac{(\lambda + \mu_+)}{2(\mu_+ - \mu_-)}(kr - b/a)e^{\mu_- \Delta}, \tag{A.19}$$

$$c_1 = b_1 + b_2, \tag{A.20}$$

and

$$\Delta = \frac{1}{\mu_+ - \mu_-} \log\left[\frac{(\lambda + \mu_+)(\mu_- - \nu)}{(\lambda + \mu_-)(\mu_+ - \nu)}\right]. \tag{A.21}$$

Expressions (A.6)–(A.11) and (A.17)–(A.21) define the linearized solution for $M_I$. An example of such a front wave is shown in Fig. 5.

Using expressions (A.9)–(A.11) in (A.21), it is easy to find

$$\Delta = \frac{\sqrt{D}}{i\sqrt{(b-c)a(K-K_0)}} \log(w_1 w_2), \tag{A.22}$$

where

$$w_1 = \frac{\lambda + \mu_+}{\lambda + \mu_-} \equiv e^{i\phi_1}, \tag{A.23}$$

$$w_2 = \frac{\mu_- - \nu}{\mu_+ - \nu} \equiv e^{-i\phi_2}, \tag{A.24}$$

where $\phi_1$ and $\phi_2$ are respectively the arguments of the complex numbers $\lambda + \mu_+$ and $\mu_+ - \nu$. It is easy to see that $\phi_1$ and $\phi_2$ do not depend on $D$, so that the logarithm only corrects the dependence of $\Delta$ on $(b-c)a(K-K_0)$. It can be also easily observed that $w_1$ lies in the second quadrant, and $w_2$ in the fourth, and that $\Im w_1 = -\Im w_2$. When $K \to K_0^+$, the imaginary parts tend to zero and the phase difference between both tend to $\pi$. Consequently the leading behavior of $\Delta$ results:

$$\Delta \sim \sqrt{D}[(b-c)a(K-K_0)]^{-1/2}. \tag{A.25}$$

The functional dependence of $\Delta$ thus found from the piecewise linearization agrees with that found numerically in the nonlinear system. The exponent $-0.388$ of the numerical results, however, is not correctly predicted by this linearization.

## REFERENCES

Abramson, G., A. R. Bishop and V. M. Kenkre (2001). Effects of transport memory and nonlinear damping in a generalized Fisher's equation. *Phys. Rev. E* **64**, 066615-1-6.

Abramson, G. and V. M. Kenkre (2002). Spatio-temporal patterns in the hantavirus infection. *Phys. Rev. E* **66**, 011912-1-5.

Childs, J. E. *et al*. (1994). Serologic and genetic identification of Peromyscus maniculatus as the primary rodent reservoir for a new hantavirus in the southwestern United States. *J. Infect. Dis.* **169**, 1271–1280.

Ernest, S. K. M., J. H. Brown and R. R. Parmenter (2000). Rodents, plants, and precipitation: spatial and temporal dynamics of consumers and resources. *Oikos* **88**, 470–482.

Fisher, R. A. (1937). The wave of advance of advantageous genes. *Ann. Eugenics* **7**, 355–369.

Mills, J. N., T. G. Ksiazek, C. J. Peters and J. E. Childs (1999a). Long-term studies of hantavirus reservoir populations in the southwestern United States: a synthesis. *Emerging Infect. Dis.* **5**, 135–142.

Mills, J. N., T. L. Yates, T. G. Ksiazek, C. J. Peters and J. E. Childs (1999b). Long-term studies of hantavirus reservoir populations in the southwestern United States: rationale, potential, and methods. *Emerging Infect. Dis.* **5**, 95–101.

Murray, J. D. (1993). *Mathematical Biology*, 2nd edn, New York: Springer.

Nichol, S. T., C. F. Spiropoulou, S. Morzunov, P. E. Rollin, T. G. Ksiazek, H. Feldmann, A. Sanchez, J. Childs, S. Zaki and C. J. Peters (1993). Genetic identification of a hantavirus associated with an outbreak of acute respiratory illness. *Science* **262**, 914–917.

Parmenter, R. R., J. W. Brunt, D. I. Moore and E. S. Morgan (1993). *The Hantavirus Epidemic in the Southwest: Rodent Population Dynamics and the Implications For Transmission of Hantavirus-associated Adult Respiratory Distress Syndrome (HARDS) in the Four Corners Region*. Sevilleta LTER Publication No. 41, pp. 1–45.

Parmenter, C. A., T. L. Yates, R. R. Parmenter and J. L. Dunnum (1999). Statistical sensitivity for detection of spatial and temporal patterns in rodent population densities. *Emerging Infect. Dis.* **5**, 118–125.

Parmenter, C. A., T. L. Yates, R. R. Parmenter, J. N. Mills, J. E. Childs, M. L. Campbell, J. L. Dunnum and J. Milner (1998). Small mammal survival and trapability in mark-recapture monitoring programs for hantavirus. *J. Wildl. Dis.* **34**, 1–12.

Stickel, L. F. (1968). Home range and travels, in *Biology of Peromyscus (Rodentia)*, Special publication No. 2, J. A. King (Ed.), Stillwater, Oklahoma: The American Society of Mammalogists, pp. 373–411.

Terman, C. R. (1968). Population dynamics, in *Biology of Peromyscus (Rodentia)*, Special publication No. 2, J. A. King (Ed.), Stillwater, Oklahoma: The American Society of Mammalogists, pp. 412–450.

Vessey, S. H. (1987). Long-term population trends in white-footed mice and the impact of supplemental food and shelter. *Am. Zoologist* **27**, 879–890.

Yates, T. L. *et al*. (2002). The ecology and evolutionary history of an emergent disease: hantavirus pulmonary syndrome. *Bioscience* **52**, 989–998.

*Received 30 July 2002 and accepted 16 January 2003*